Superconducting dome revealed by surface structure dependence in single unit cell FeSe on $SrTiO_3$(001)

Tomoaki Tanaka,[1,*] Kenta Akiyama,[1] Satoru Ichinokura,[1] Ryota Shimizu,[2] Taro Hitosugi,[2] and Toru Hirahara[1]
[1]*Department of Physics, Tokyo Institute of Technology, Tokyo 152-8551, Japan*
[2]*School of Materials and Chemical Technology, Tokyo Institute of Technology, Tokyo 152-8550, Japan*

(Received 27 November 2019; accepted 4 May 2020; published 20 May 2020)

We report the superconducting properties of single unit cell FeSe prepared on $SrTiO_3$ (STO) (001)-$c(6 \times 2)$ using scanning tunneling microscopy/spectroscopy (STM/STS). A surface superstructure of $c(6 \times 2)$ was obtained by annealing the substrate under an oxygen atmosphere. A 3×1 periodicity, which corresponds to the topmost Ti atoms of the substrate, was observed in high-resolution STM images, and the superconducting gap size was 11.5 ± 2.5 meV. A nonsuperconducting region with additional $\sqrt{2} \times \sqrt{2}$ periodicity was also found, and this originates from the difference in the arrangement of the Sr and Ti atoms at the surface. We conclude that there is a universal superconducting dome structure in the (electron-doping level)—(superconducting gap size) phase diagram by comparing with previous results that controlled the surface of the substrate/film and the gap size can be maximized/minimized by selecting the appropriate STO surface superstructure.

DOI: 10.1103/PhysRevB.101.205421

I. INTRODUCTION

A single unit cell (1UC) FeSe film grown on $SrTiO_3$(001) (STO) has attracted great attention because its T_C rises to 60–109 K [1–3], much higher than that of the bulk (8 K) [4]. The electron doping due to band bending or from oxygen vacancies of the STO surface or by foreign atom deposition on FeSe is considered to be the most important factor [5,6], although there are conflicting results showing that the electron doping will suppress/enhance superconductivity for large doping [7,8]. Contradictory reports on the undoped parent phase (insulator [9] or Dirac semimetal with weak metallicity [10]) have also been reported. The coupling between optical surface phonons of the STO and electrons in FeSe has been proposed as another important factor [8,11].

In any case, the interface between 1UC FeSe and STO should play an important role. At this interface, a superstructure of the STO surface exists. Different structures of the STO surface have been reported [12–19] due to the variation in the amount of oxygen deficiencies [18] as well as the different terminations (TiO_2 and SrO) [19]. It can be imagined that the difference in the surface superstructures should change the electron doping to FeSe. However, this has been overlooked, and only few studies have focused on this point. We previously investigated the superconducting properties of 1UC FeSe deposited on the STO-2×1 and $\sqrt{2} \times \sqrt{2}$ [20]. We found that the superconducting gap size depends on the superstructure although a microscopic explanation was not given.

Therefore, in this paper, we aimed to investigate the effect of electron doping from the STO surface in more detail. For this purpose, the $c(6 \times 2)$ surface was prepared by annealing the substrate under an oxygen atmosphere to reduce the oxygen vacancies. From high-resolution scanning tunneling microscopy/scanning tunneling spectroscopy (STM/STS) measurements, we found that 1UC FeSe/STO-$c(6 \times 2)$ was superconducting with a gap size of 11.5 ± 2.5 meV. A 3×1 periodicity was observed, reflecting the periodicity of the topmost Ti atoms of the $c(6 \times 2)$ surface. In addition, a nonsuperconducting region with additional $\sqrt{2} \times \sqrt{2}$ periodicity coexisted. This likely originates from the difference in the local arrangement of the surface atoms. By comparing with our previous results [20], it was found that the amount of electron doping to FeSe differs depending on the STO surface reconstruction and the superconducting gap size changes accordingly. Furthermore, taking into account the previous results that have controlled the electron doping with FeSe surface adsorption [7,21], we found clear evidence of a universal superconducting dome structure and an optimal doping level in 1UC FeSe/STO. This undoubtedly shows the importance to control the STO surface in this system.

II. RESULTS AND DISCUSSIONS

Nb-doped STO substrates (Shinkosha, 0.05 wt %) were used in this paper. To make a surface with fewer oxygen vacancies than 2×1 and $\sqrt{2} \times \sqrt{2}$, the substrate was treated under an oxygen atmosphere which is described by P_{O_2}. After degassing a STO substrate at 500 °C for 2 h at $P_{O_2} = 1 \times 10^{-6}$ Torr, we heated the STO at 850 °C for 30 min and, then, at $T_{max} = 1130$ °C for 3 min at $P_{O_2} = 1 \times 10^{-5}$ Torr [17]. We found a bright reflection high-energy electron diffraction (RHEED) pattern as shown in Fig. 1(a). It suggests that the surface superstructure is $c(6 \times 2)$. Figure 1(b) shows the STM image. The white lines in Fig. 1(b) show the STO step, and it indicates that the STO has a step-terrace structure. The evolution of the RHEED patterns and STM images for different T_{max}'s is shown in Fig. S1 of the Supplemental Material [22]. After the STO surface was cleaned, Fe (99.5%) and Se (99.999%) with a flux ratio of ~1:5 were coevaporated

*tanaka@surfnano.phys.titech.ac.jp

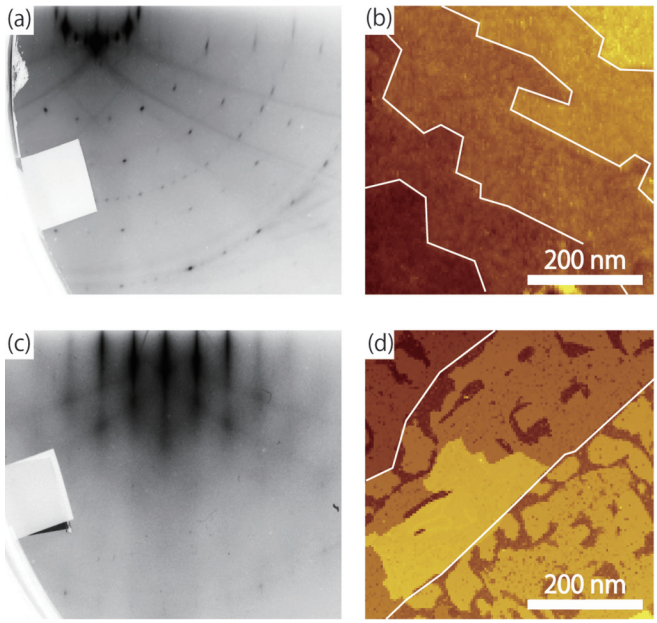

FIG. 1. (a) and (c) RHEED patterns of STO (001)-$c(6 \times 2)$ and a 1UC FeSe film deposited on the STO surface shown in (a), respectively. Electrons are incident from the [100] direction. (b) and (d) Topographic images (500×500 nm^2) measured for samples (a) and (c), respectively. The white lines show the atomic step of STO.

at a substrate temperature of 480 °C followed by annealing at the same temperature for 30 min [23]. The RHEED shows the 1×1 pattern of FeSe and reveals the growth of a high quality film [Fig. 1(c)]. The thickness was monitored with RHEED oscillations. Then, the samples were transferred to the STM/STS system (Unisoku, USM1500). The measurements were performed at 5 K with a PtIr tip. The dI/dV spectra were acquired using the lock-in technique with a bias modulation (measured near Fermi level: 1 mV and the others: 5 mV) at 1093 Hz. Figure 1(d) shows the STM image of the grown samples, showing a flat film formation.

Figure 2(a) shows the same picture with the morphology indicated. This was derived from Fig. 2(b) showing the line profile obtained along the blue arrow in Fig. 2(a) and considering the known height of a single step for FeSe (~0.55 nm) and STO (~0.39 nm). There are three distinct regions: 1UC, 2UC FeSe, and the bare STO [see also the schematic in the inset of Fig. 2(b)]. For 1UC FeSe, there are two types of domains: unisolated ones which extend over 200 nm and isolated ones which are surrounded by the bare STO near the step edges. We will call the unisolated (isolated) region 1UC FeSe $A(B)$. Figure 2(c) shows the STS spectra of 1UC FeSe. The peak position of the valence band is different between the two (A: -0.17 eV and B: -0.48 eV). It clearly shows that the electronic structure of the two domains is different.

To get further insight into this difference, we measured bias-dependent atomically resolved topographic images as shown in Figs. 2(d) and 2(e) for domain A and 2(f) and 2(g) for domain B. All the images show a 3×1 periodicity as indicated by the blue arrows. In addition, there seems to be another order in Fig. 2(g). The insets show the fast Fourier Transformation (FFT) images to show this periodicity more

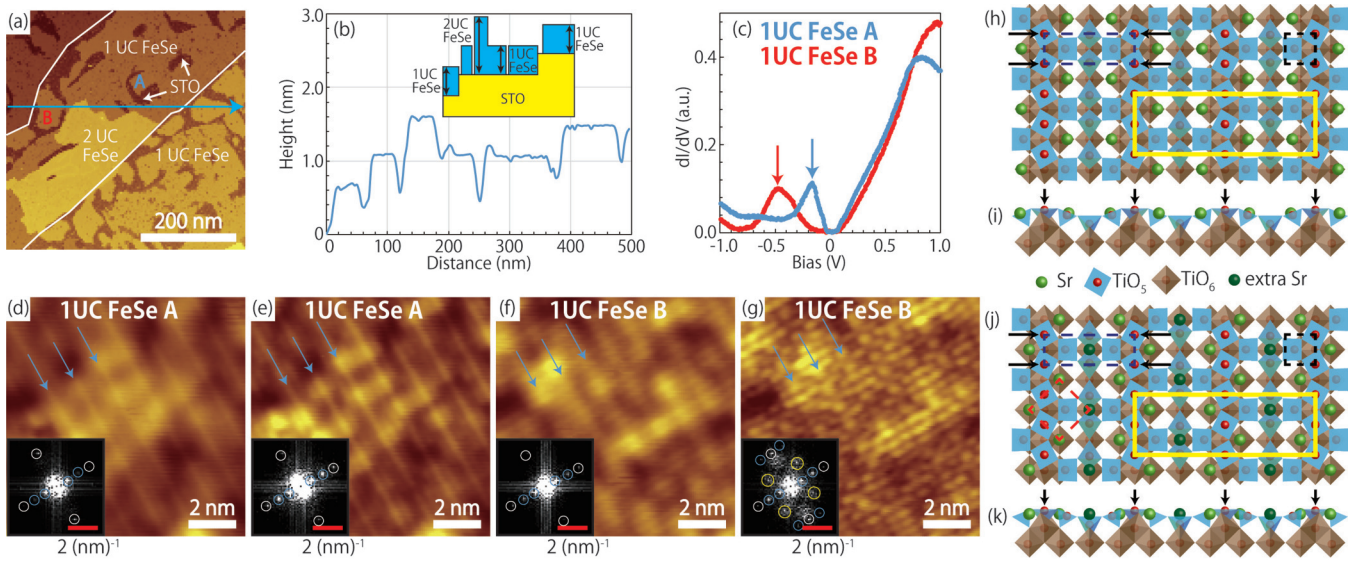

FIG. 2. (a) A topographic image of 1UC FeSe on STO (001)-$c(6 \times 2)$ after optimum annealing. (b) Line profile along the blue arrow in (a). The inset shows the schematic of the surface morphology. (c) dI/dV spectra taken on 1UC FeSe A and B in (a) (1.0 V, 300 pA). (d) and (e) Enlarged topographic images obtained for 1UC FeSe A [10 nm $\times$ 10 nm, 110 pA, (d) 200 mV, and (e) 100 mV]. (f) and (g) Enlarged topographic images obtained for 1UC FeSe B [10 nm $\times$ 10 nm, 110 pA, (f) 200 mV, and (g) 100 mV]. The blue arrows represent the 3×1 periodicity. The insets show fast Fourier transform (FFT) images. The white, blue, and yellow circles represent the periodicities of 1×1, 3×1, and $\sqrt{2} \times \sqrt{2}$, respectively. (h) Structure model of STO-$c(6 \times 2)$ as proposed in Ref. [16]. Sr and Ti atoms are represented by green and red spheres. Brown and blue units are TiO_6 and TiO_5, respectively. The black dashed square and the blue dashed rectangle represent the 1×1 and the 3×1 periodicities, respectively. The unit cell $c(6 \times 2)$ is shown by the yellow solid rectangle. Topmost Ti atoms are indicated by black arrows. (i) Side view of (h). (j) Structure model of $c(6 \times 2)$ with additional Sr atoms (dark green spheres) to form the $\sqrt{2} \times \sqrt{2}$ periodicity (red dashed square). (k) Side view of (j).

clearly. The white, blue, and yellow circles represent the periodicities of 1×1, 3×1, and $\sqrt{2} \times \sqrt{2}$, respectively (For the details of the FFT images, refer to Figs. S3, S4, and S7 of the Supplemental Material [22]). Thus, we can say that there is a $\sqrt{2} \times \sqrt{2}$ periodicity in domain B which is absent in domain A.

First, we will discuss the origin of this 3×1 periodicity. We have previously reported that the STO surface periodicity can be imaged through the 1UC FeSe film [20] and this is also supported in the literature [5,24]. Thus, the $c(6 \times 2)$ periodicity should be observed for the present samples not 3×1. Figures 2(h) and 2(i) show the reported structure model of STO-$c(6 \times 2)$ [16]. The black square and yellow rectangle represent the 1×1 and $c(6 \times 2)$ periodicities, respectively. Focusing on the topmost layer of the substrate, there are Ti atoms with dangling bonds as indicated by the black arrows. If we just focus on the periodicity of these Ti atoms, it is 3×1. Thus, it can be anticipated that the electrons doped to 1UC FeSe are probably coming from these dangling bonds. Further details of the bias dependence of the atomic resolution images are shown in Fig. S2 of the Supplemental Material [22], but only Fig. 2(g) shows the additional $\sqrt{2} \times \sqrt{2}$ periodicity. It has been reported that a unidirectional 3×1 periodicity coexists with $\sqrt{2} \times \sqrt{2}$ on the Sr-rich STO(001) surface [25], and what is shown in Fig. 2(g) has the same characteristics. However, the structure shown in Fig. 2(h) does not have a $\sqrt{2} \times \sqrt{2}$ periodicity. If we include more Sr atoms and slightly change the position of the Sr atoms and TiO_5 tetrahedrons, a $\sqrt{2} \times \sqrt{2}$ periodicity can be obtained as shown in Fig. 2(j). Thus, we think that, although the unit cells of domains A and B are both $c(6 \times 2)$, the atomic arrangement at the surface is slightly different and results in the difference in the electronic structure revealed in Fig. 2(c). The possible origin of this difference in the context of the evaporation of Sr is discussed in the Supplemental Material (Fig. S8) [22].

To investigate the superconducting properties, we performed STS measurements of FeSe A and B near the Fermi level as shown in Figs. 3(a) and 3(c), respectively. There is a superconducting gap for 1UC FeSe A whereas 1UC FeSe B shows an insulating gap. Similar features were observed at different regions in Fig. 2(a) (Fig. S5 of the Supplemental Material [22]). The presence/absence of the superconducting gap is most likely caused by the difference in the electronic structure as shown in Fig. 2(c) (details will be discussed later). To estimate the superconducting gap size in domain A, the spectrum was normalized using the extrapolated method [20] [Fig. 3(b)]. The coherence peaks become clearer, and the gap size is estimated as 10 meV. Figures S9 and S10 of the Supplemental Material [22] show the spatial dependence of the superconducting/insulating gap. Although the gap size slightly differs depending on the location, there is no mixing between the two within the same region. We measured more than 200 spectra at 60 different positions in domain A. Figure 3(d) shows the statistical distribution map, and the gap size is 11.5 ± 2.5 meV. We have also performed STM/STS measurements for a completely different area of the sample and found similar behavior to what are shown in Figs. 2(c), 3(a), and 3(c) (Figs. S6 and S7 of the Supplemental Material [22]). No transient region between A and B was observed. It should also be noted that the regions with insulating gaps were

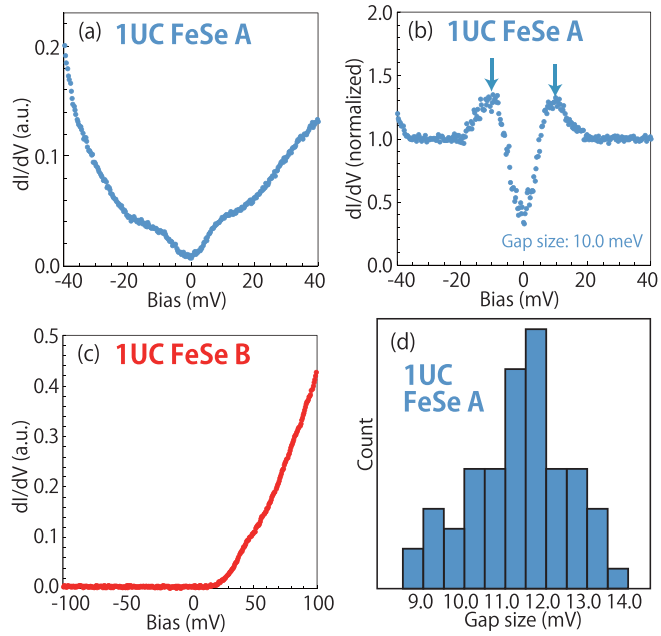

FIG. 3. (a) and (c) dI/dV spectra obtained near the Fermi level for 1UC FeSe A and B, respectively. (b) The dI/dV spectrum of the 1UC FeSe A normalized using the extrapolated method [20]. (d) Statistical analysis of the distribution of the gap size for 1UC FeSe A.

located only near the step edges. Thus, there is an interesting situation where a superconducting and a nonsuperconducting region is coexisting without intermixing due to the slight difference in the surface reconstruction for 1UC/STO $c(6 \times 2)$.

Now, we focus on the superconductivity of 1UC FeSe/STO-$c(6 \times 2)$ on the two domains (1UC FeSe A and B) as well as that for the films grown on different surface superstructures [20]. In the previous study of K adsorption on 1UC FeSe, the valence-band peak position, which corresponds to the peak in Fig. 2(c), was ~ -0.25 eV for the pristine surface, and it shifted away from the Fermi level with more K deposition. The superconducting gap size decreased accordingly [7]. K atoms were considered to dope electrons to the FeSe, and this behavior was actually detected as the change in peak position of the occupied state, which corresponds to the kink of the valence band [7,26]. This means that we can estimate the electron-doping level from the measured valence-band peak position shown in Fig. 2(c). Figure 4(a) shows its comparison for 1UC FeSe deposited on different surface superstructures of STO. The black dashed line marks the shift of the peak position for each spectrum, and we can unambiguously say that the electron doping depends on the substrate surface superstructure. Focusing on the peak of 1UC FeSe A on STO-$c(6 \times 2)$, it is the closest to the Fermi level. This means that we have successfully created a STO surface with less oxygen vacancies. On the contrary, the peak position of 1UC FeSe B is the farthest from the Fermi level. Although the domain size of domain B is a bit small, the quantum size effect is not important since it is larger than 200 nm^2 [20,27]. We believe that there is more doping in domain B due to the extra Sr atoms by comparing Figs. 2(h) and 2(j) as there are no O atoms to make a chemical bond for them. The fact

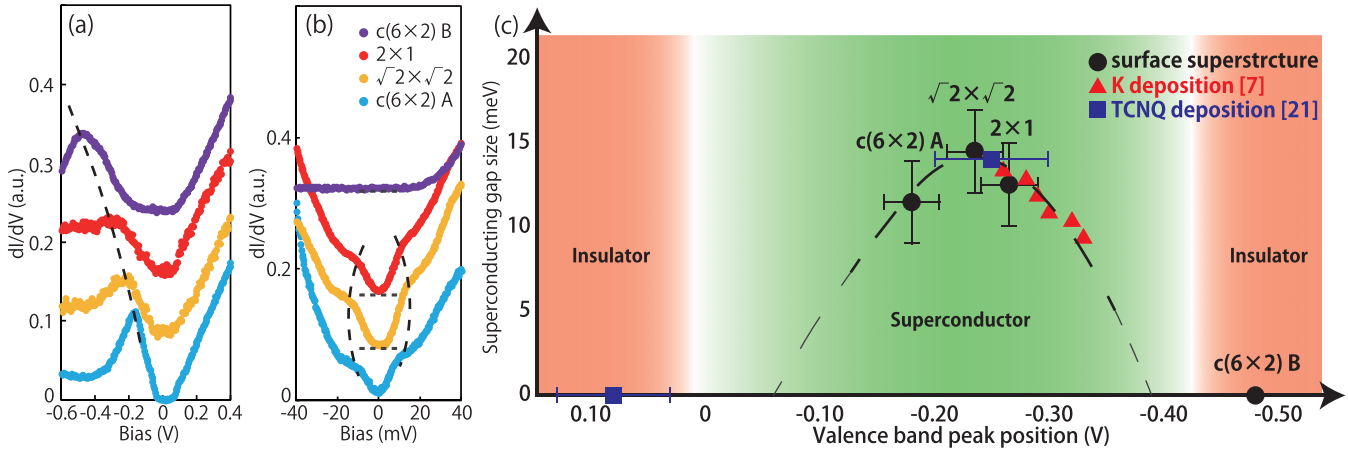

FIG. 4. (a) and (b) dI/dV spectra taken on the 1UC FeSe grown on different surface superstructures [2×1, $\sqrt{2} \times \sqrt{2}$, and $c(6 \times 2)$] and those obtained near the Fermi level showing the gap, respectively. (c) Phase diagram of the peak position and the superconducting gap size measured for 1UC FeSe samples grown on several surface superstructures (black), electron doped with K adsorption (red) [7], and hole doped with 7,7,8,8-tetracyanoquinodimethane (TCNQ) deposition (blue) [21], respectively. The error bars were determined from histograms made from position-dependent measurements, such as the one shown in Fig. 3(d).

that the $\sqrt{2} \times \sqrt{2}$ periodicity appeared through the 1UC FeSe supports this hypothesis.

Figure 4(b) compares the STS spectra of the superconducting gap for the samples shown in Fig. 4(a). The gap size is clearly different as shown by the black dashed line. This undoubtedly reveals that the electron-doping level depends on the surface superstructure, and the gap size changes accordingly. To see this relationship more clearly, a correlation diagram between the electron-doping level (the valence-band peak position) and the gap size is shown in Fig. 4(c). The black circles represent our data points for various surface superstructures. We have also plotted this relationship for the K-deposited electron-doping [7] (red triangles) and TCNQ-deposited hole-doping [21] cases (blue rectangles) [22]. The superconducting gap size decreases monotonously with more K doping. It is consistent with the difference in 2×1 and $\sqrt{2} \times \sqrt{2}$ surface structures. For the low-doped side, the TCNQ hole-doped sample does not show superconductivity and is insulating since it is heavily hole doped. One can unambiguously say that there is a universal superconducting dome structure independent of the doping method.

There is, in fact, another paper that has discussed the low-doping side [9]. By changing the annealing condition of the as-grown FeSe films, the excess Se amount was controlled, and an insulator-to-superconductor transition was shown to occur. However, it only revealed an increase in the gap size and T_C without reaching the optimal or overdoped regions. By combining our present results with previous STM/STS reports of surface adsorption, we can be sure that the substrate surface can influence the electron doping. When the adsorbed atoms/molecules are used as dopants, they are carrier scatterers at the same time. On the other hand, carrier tuning with surface superstructures does not likely induce additional scattering, and this should be an advantage in transport measurements.

Let us now discuss the controversy of the undoped parent phase. In Ref. [9], it was discussed whether the parent insulating phase of as-grown 1UC FeSe was a result of Anderson localization or a Mott insulator. Since we can exclude the role of disorder in the present samples with controlled superstructures, our results favor the Mott insulating state as the undoped phase. However, since it is difficult to define the undoped sample in reality, we cannot completely deny that it is metallic. One may be able to say that the sample in Ref. [10] claiming the Dirac semimetal state does not really correspond to the undoped phase since it was already annealed mildly. Further study is needed to elucidate the true nature of the parent phase as both Refs. [9,10] suggest that correlation effects are enhanced by the reduced dimensionality.

III. CONCLUSION

To summarize, we succeeded in fabricating the STO(001)-$c(6 \times 2)$ surface and measured the superconductivity properties of 1UC FeSe grown on it with high-resolution STM/STS. We were able to obtain the atomic resolution image with a 3×1 periodicity, which originates from the dangling bond of the Ti atoms of the $c(6 \times 2)$ surface. The superconducting gap size was 11.5 ± 2.5 meV. In addition, there were nonsuperconducting regions that correspond to regions with different surface reconstructions formed locally. Combining with previous reports, we found that the superconducting properties universally change with the amount of electron doping, and a dome structure in the phase diagram was obtained. Our result clearly reveals the superconducting properties can be optimized by preparing the proper surface.

ACKNOWLEDGMENT

This work has been supported by Grants-in-Aid from the Japan Society for the Promotion of Science (Grants No. 15H05453, No. 16K13683, and No. 18H03877), the Toray Science Foundation (Grant No. 14-5508), and the Research Support Grant (B) of Tokyo Institute of Technology.

[1] Q.-Y. Wang, Z. Li, W.-H. Zhang, Z.-C. Zhang, J.-S. Zhang, W. Li, H. Ding, Y.-B. Ou, P. Deng, K. Vhang, J. Wen, C.-L. Song, K. He, J.-F. Jia, S.-H. Ji, Y.-Y. Wang, X. Chen, X.-C. Ma, and Q.-C. Xue, Chin. Phys. Lett. **29**, 037402 (2012).

[2] S. Tan, Y. Zhang, M. Xia, Z. Ye, F. Chen, X. Xie, R. Peng, D. Xu, Q. Fan, H. Xu, J. Jiang, T. Zhang, X. Lai, T. Xiang, J. Hu, B. Xie, and D. Feng, Nature Mater. **12**, 634 (2013).

[3] J.-F. Ge, Z.-L. Liu, C. Liu, C.-L. Gao, D. Zian, Q.-K. Xue, Y. Liu, and J.-F. Jia, Nature Mater. **14**, 285 (2014).

[4] F.-C. Hsu, J.-Y. Luo, K.-W. Yeh, T.-K. Chen, T.-W. Huang, P. M. Wu, Y.-C. Lee, Y.-L. Huang, Y.-Y. Chu, D.-C. Yan, and M.-K. Wu, Proc. Natl. Acad. Sci. USA **105**, 14262 (2008).

[5] J. Bang, Z. Li, Y. Y. Sun, A. Samanta, Y. Y. Zhang, W. Zhang, L. Wang, X. Chen, X. Ma, Q.-K. Xue, and S. B. Zhang, Phys. Rev. B **87**, 220503(R) (2013).

[6] H. Ding, Y.-F. Lv, K. Zhao, W. L. Wang, L. Wang, C.-L. Song, X. Chen, X.-C. Ma, and Q.-K. Xue, Phys. Rev. Lett. **117**, 067001 (2016).

[7] C. Tang, D. Zhang, Y. Zang, C. Liu, G. Zhou, Z. Li, C. Zheng, X. Hu, C. Song, S. Ji, K. He, X. Chen, L. Wang, X. Ma, and Q.-K. Xue, Phys. Rev. B **92**, 180507(R) (2015).

[8] X. Shi, Z.-Q. Han, X.-L. Peng, P. Richard, T. Qian, X.-X. Wu, M.-W. Qiu, S. C. Wang, J. P. Hu, Y.-J. Sun, and H. Ding, Nat. Commun. **8**, 14988 (2017).

[9] J. He, X. Liu, W. Zhang, L. Zhao, D. Liu, S. He, D. Mou, F. Li, C. Tang, Z. Li, L. Wang, Y. Peng, Y. Liu, C. Chena, L. Yu, G. Liu, X. Dong, J. Zhang, C. Chen, Z. Xu, X. Chen, X. Ma, Q. Xue, and X. J. Zhou, Proc. Natl. Acad. Sci. USA **111**, 18501 (2014).

[10] S. Kanayama, K. Nakayama, G. N. Phan, M. Kuno, K. Sugawara, T. Takahashi, and T. Sato, Phys. Rev. B **96**, 220509(R) (2017).

[11] J. J. Lee, F. T. Schmitt, R. G. Moore, S. Johnston, Y.-T. Cui, W. Li, M. Yi, Z. K. Liu, M. Hashimoto, Y. Zhang, D. H. Lu, T. P. Devereaux, D.-H. Lee, and Z.-X. Shen, Nature (London) **515**, 245 (2014).

[12] Q. D. Jiang and J. Zegenhagen, Surf. Sci. **425**, 343 (1999).

[13] M. R. Castell, Surf. Sci. **505**, 1 (2002).

[14] T. Kubo and H. Nozoye, Surf. Sci. **542**, 177 (2003).

[15] M. Naito and H. Sato, Physica C **229**, 1 (1994).

[16] J. Ciston, H. G. Brown, A. J. D'Alfonso, P. Koirala, C. Ophus, Y. Lin, Y. Suzuki, H. Inada, Y. Zhu, L. J. Allen, and L. D. Marks, Nat. Commun. **6**, 7358 (2015).

[17] R. Shimizu, K. Iwaya, T. Ohsawa, S. Shiraki, T. Hasegawa, T. Hashizume, and T. Hitosugi, ACS Nano **5**, 7967 (2011).

[18] R. Shimizu, K. Iwaya, T. Ohsawa, S. Shiraki, T. Hasegawa, T. Hashizume, and T. Hitosugi, Appl. Phys. Lett. **100**, 263106 (2012).

[19] S. Ogawa, K. Kato, N. Nagatsuka, S. Ogura, and K. Fukutani, Phys. Rev. B **96**, 085303(R) (2017).

[20] T. Tanaka, K. Akiyama, and R. Yoshino, and T. Hirahara, Phys. Rev. B **98**, 121410(R) (2018).

[21] J. Guan, J. Liu, B. Liu, X. Huang, Q. Zhu, X. Zhu, J. Sun, S. Meng, and W. Wang, and J. Guo, Phys. Rev. B **95**, 205405 (2017).

[22] See Supplemental Material at http://link.aps.org/supplemental/10.1103/PhysRevB.101.205421 for the additional information about the contents of this article that show complementary data of STM/STS measurements and details about statements written in the main text.

[23] We found that the substrate temperature of 480 °C was the optimum for the FeSe growth on STO-$c(6 \times 2)$.

[24] Z. Li, J.-P. Peng, H.-M. Zhang, W.-H. Zhang, H. Ding, P. Deng, K. Chang, C.-L. Song, S.-H. Ji, L. Wang, K. He, X. Chen, Q.-K. Xue, and X.-C. Ma, J. Phys.: Condens. Matter **26**, 265002 (2014).

[25] K. Iwaya, R. Shimizu, T. Ohsawa, T. Hashizume, and T. Hitosugi, Phys. Rev. B **83**, 125117 (2011).

[26] I. A. Nekrasov, N. S. Pavlov, and M. V. Sadovskii, J. Exp. Theor. Phys. **126**, 485 (2018).

[27] Z. Li, J.-P. Peng, H.-M. Zhang, C.-L. Song, S.-H. Ji, L. Wang, K. He, X. Chen, Q.-K. Xue, and X.-C. Ma, Phys. Rev. B **91**, 060509(R) (2015).